Icarus 305 (2018) 84–90

Contents lists available at ScienceDirect

Icarus

journal homepage: www.elsevier.com/locate/icarus

Atmospheric dynamics and habitability range in Earth-like aquaplanets obliquity simulations

Priscilla Nowajewski[a,b,*], M. Rojas[b], P. Rojo[c], S. Kimeswenger[a,d]

[a] Instituto de Astronomía, Universidad Católica del Norte, Av. Angamos 0610, Antofagasta, Chile
[b] Departamento de Geofísica, Universidad de Chile, Blanco Encalada 2002, Santiago de Chile, Chile
[c] Departamento de Astronomía, Universidad de Chile, Casilla 36-D, Santiago de Chile, Chile
[d] Institut für Astro- und Teilchenphysik, Universität Innsbruck, Technikerstr. 25, 6020 Innsbruck, Austria

ARTICLE INFO

Article history:
Received 5 September 2017
Revised 14 December 2017
Accepted 2 January 2018
Available online 6 January 2018

Keywords:
Astrobiology
Atmospheres
Dynamics
Atmospheres
Evolution
Geophysics
Meteorology
Terrestrial planets

ABSTRACT

We present the evolution of the atmospheric variables that affect planetary climate by increasing the obliquity by using a general circulation model (PlaSim) coupled to a slab ocean with mixed layer flux correction.

We increase the obliquity between 30° and 90° in 16 aquaplanets with liquid sea surface and perform the simulation allowing the sea ice cover formation to be a consequence of its atmospheric dynamics.

Insolation is maintained constant in each experiment, but changing the obliquity affects the radiation budget and the large scale circulation. Earth-like atmospheric dynamics is observed for planets with obliquity under 54°. Above this value, the latitudinal temperature gradient is reversed giving place to a new regime of jet streams, affecting the shape of Hadley and Ferrel cells and changing the position of the InterTropical Convergence Zone.

As humidity and high temperatures determine Earth's habitability, we introduce the wet bulb temperature as an atmospheric index of habitability for Earth-like aquaplanets with above freezing temperatures. The aquaplanets are habitable all year round at all latitudes for values under 54°; above this value habitability decreases toward the poles due to high temperatures.

1. Introduction

The obliquity of a planet is the angle between its spin and orbital angular momentum vectors. It is one of the parameters which determine planetary climate.

Bodies with high obliquity are not a rarity in our solar system. Venus has an obliquity of 0° with retrograde rotation. Neptune and Uranus have inclinations of 30° and ≈90° respectively, whereas Pluto has an obliquity of 54° with retrograde rotation (Dobrovolskis and Harris, 1983). Among these values, 54° of obliquity has a special geometrical meaning since the planet receives the same insolation over a year at the equator and the poles. This means that in such a planet there is believed to be no energy transport, being in dynamic equilibrium at this angle.

The value of obliquity can be chaotic due to external and internal forces acting on the planet (Laskar and Robutel, 1993). E.g. the obliquity of Mars varies between 0° and 60° in a period of 100 000 years (Touma and Wisdom, 1993; Bills, 1990), while the Earth's obliquity varies on a small range between 22° and 24° every 41 000 years. Currently, the Earth has an obliquity of 23.5° on its increasing path (Berger and Loutre, 1991). This relative stability of the Earth's obliquity is the result of the tidal effect of the Moon (Laskar et al., 1993). This stability results in small latitudinal variations in the distribution of the incoming radiation at the top of the atmosphere, thereby keeping a stable climate essential for the proliferation of life. These small variations, together with changes in the other orbital parameters, are however important enough to produce significant climatic variations, such as the glacial-interglacial cycles, prevalent in the Earth's climate over the last two million years approximately (Imbrie et al., 1993).

Even when the evidence of these small variations exists, Jenkins (2000) searched an explanation for the faint young sun paradox (Sagan and Mullen, 1972) and low latitude glaciation (Hoffman, 1998) that occurred late in the Precambrian period (from 4600 to 540 million years ago), through an Earth with an obliquity of 70°.

The minimum condition for planetary habitability is the presence of liquid water on its surface. In most cases this is determined by the distance between the planet and its host star (Kopparapu et al., 2013). However a planet can be partially hab-

* Corresponding author at: Instituto de Astronomía, Universidad Católica del Norte, Av. Angamos 0610, Antofagasta, Chile.
E-mail address: pnowajew@dgf.uchile.cl (P. Nowajewski).

https://doi.org/10.1016/j.icarus.2018.01.002
0019-1035/

itable depending on the amount of sea ice cover, but also on its continental distribution (Williams and Kasting, 1997; Spiegel et al., 2009; Williams and Pollard, 2003), and its surface temperatures which must be cool enough to avoid a runaway greenhouse effect (Kasting, 1988; Sugiyama et al., 2005; Spiegel et al., 2008).

Atmospheric dynamics also influences the state of water at the surface of a planet. Furthermore, atmospheric humidity and air temperature play a key role for habitability as quantified by Sherwood and Huber (2010). They tested the terrestrial habitability in a future scenario of climate change using the wet bulb temperature (T_w), which corresponds to the lowest temperature that can be reached by evaporating all its moisture (North and Erukhimova, 2009). In particular, mammals are only able to survive in regions where T_w is below 35°C. Above this limit, the body loses the ability to dissipate metabolic heat, inducing hyperthermia (death by high temperatures).

We study the response of an Earth-like aquaplanet (planets with similar orbital and physical parameters as Earth but without continents) only to changes in obliquity. We do not discuss the effects of continental distribution or other variables that can influence habitability (Williams and Kasting, 1997; Spiegel et al., 2009; Williams and Pollard, 2003).

Aquaplanet simulations are simplified experiments to explore the climate responses ignoring zonal asymmetries introduced by continents (Williamson et al., 2013). Aquaplanet configurations have been used to study the influence of obliquity on planets climate before (Linsenmeier et al., 2015; Kilic et al., 2017), and compared to Earth's current obliquity value. Most of these studies were carried out with atmospheric models and a slab ocean, therefore focusing on the role of the atmosphere in the heat transport. Ferreira et al. (2014) using a coupled Atmosphere-Ocean General Circulation Model (A-OGCM) in aquaplanet mode found that the ocean of an aquaplanet with 90° of obliquity turns into a heat reservoir, maintaining warm temperatures even at the hemisphere that is in complete darkness, similar to slab ocean results.

The effects over climate at extreme obliquities (0°, 54° and 90°) are usually compared with Earth's current obliquity value (Ferreira et al., 2014; Jenkins, 2000; Williams and Pollard, 2003). It is also assumed that atmospheric variables follow the same transition observed at 54° of obliquity in the insolation (Ward, 1974), although Linsenmeier et al. (2015) used 55°. In this study we present 16 Earth-like aquaplanets simulations at different obliquities (from 30° to 90°, most of them have not been studied before) with a finer sampling around 55°, including the critical obliquity of 54°. This allows us to derive with higher accuracy changes in atmospheric variables that are important for planetary habitability and it allow us also to establish equations for surface temperature and precipitable water.

We study the effect on atmospheric dynamics of changing obliquity in Earth-like aquaplanets with all seasons ice-free initial conditions. The evolution of the variables that determine the heat distribution in the planet's atmosphere are analysed. For this purpose, we use an intermediate complexity model with mixed layer flux correction that simulates the oceanic heat flux. This differentiates our simulations from those of Linsenmeier et al. (2015), because they did not use oceanic heat flux, and from those of Ferreira et al. (2014), who used a dynamical ocean model. Finally, we present the role of the atmospheric effect on habitability and introduce the wet bulb temperature as an atmospheric index of habitability.

Details of the simulations and the parameters used in the simulations are presented in Section 2. In Section 3 we present the results of the experiments, including a description of the evolution of the atmospheric variables that affect the state of water over the surface of this aquaplanets. We discuss the results and give our conclusions in Section 4.

Table 1
Model parameters used in simulations.

Parameters	Symbol	Value	Units
Planet's radius	R	6300	km
Acceleration of gravity	g	9.8	m s^{-2}
Obliquity	δ	30, 40, 45,47.5,50, 52.5,54,55, 57,57.5,60, 62.5,65,70, 80,90	degrees
Eccentricity	ε	0	
Ocean depth		50	m
Simulation length		80	years
CO_2 concentration		360	ppm
Solar constant	S_0	1365	W m^{-2}
Albedo		0.06	
Distance from star		1	AU

2. Methodology

We performed sixteen Earth-like aquaplanets simulations with current Earth atmospheric composition and one current Earth simulation used to make an habitability comparison in section (3.6), using the general atmospheric circulation model Planet Simulator (PlaSim, v16.022, Fraedrich et al., 2005). Refer to the methodology section of Linsenmeier et al. (2015) for a more extensive description of this model.

PlaSim is run with spatial resolution T42 ($2.8° \times 2.8°$) using 10 vertical levels from 1000 hPa to 100 hPa (from surface to lower stratosphere). PlaSim includes sea-ice-atmosphere interaction and a slab ocean with fixed depth. We use a mixed layer flux correction that corresponds to the oceanic heat flux of the slab ocean.

We calculate the global mean surface temperature for each experiment to verify the stability of the simulations in a period of 80 years. Results stabilize and converge after 50 years. Thus, the climatology in each experiment is calculated with the final 30 years. Months have equal length of 30 days. Our aquaplanets have circular orbits (eccentricity $\varepsilon = 0$), and the obliquity (δ) changes between 30° and 90° with a finer sampling around 55° (See Table 1).

We adopted an oceanic albedo of 0.06 (Payne, 1972), and initial surface temperature above 0°C at the poles to ensure that ice will only form as a result of atmospheric dynamics and not because of the initial conditions of the simulation. We selected only $\delta \geq 30°$ because our aquaplanets with lesser obliquity run into a snowball state. Parameters used in the experiments are shown in Table 1.

As the eccentricity is neglected, the north–south symmetry holds for all experiments, therefore the analysis is presented for the Northern hemisphere only.

The grid of the model was used to define the polar region between latitudes 87.8°N and 71.9°N and the equatorial region as 1.4°N and 4.2°N. This ensures equivalent areas $\approx 0.3\,sr$ for both regions to calculate the equator to pole differences.

ΔR is defined as the insolation difference:

$$\Delta R = R_{eq} - R_{pol}, \tag{1}$$

where R_{eq} is the insolation of the equatorial area and R_{pol} is the insolation of the polar region. Both regions correspond to the latitudinal bands previously defined. ΔT is defined equivalently for surface temperature differences.

To predict the amount of precipitable water vapour content as function of the global surface temperature we used the Clausius–Clapeyron equation as inferred by Stephens (1990):

$$PWV = 10.82 \left(\frac{r}{1+\lambda}\right) e^{a(\mathrm{SST}-288)}, \tag{2}$$

where PWV is the precipitable water content in g cm^{-2} and SST is sea surface temperature in K, with values above 288 K and $a \approx$

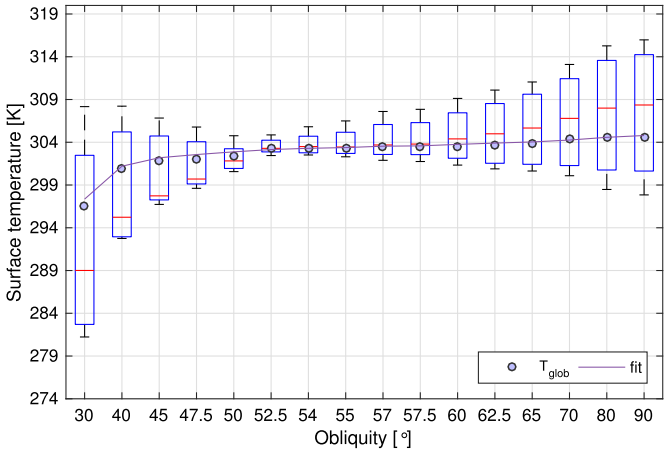

Fig. 1. Global mean surface temperature for each obliquity. Boxplots show variations in latitudinal distribution and interannual variability of surface temperatures. Red line corresponds to the median of the data, grey dots shows T_{glob}. Box extremes correspond to the lower and upper quartile. Whiskers show minimum and maximum values. Grey line is the fitting curve for T_{glob} given by Eq. (3). Note that the distance between boxplots is not linear. (For interpretation of the references to color in this figure legend, the reader is referred to the web version of this article.)

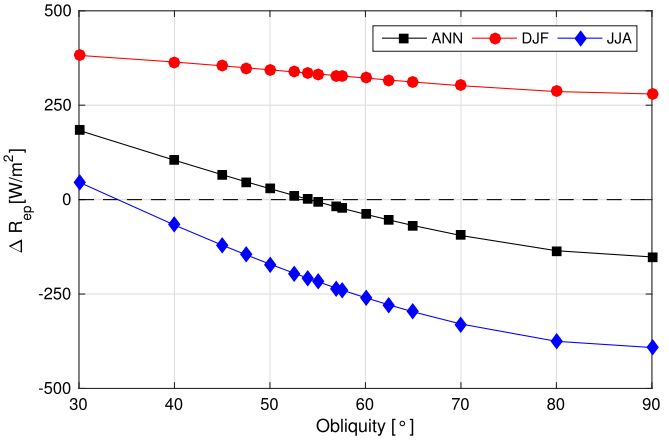

Fig. 2. Equator to pole difference of incoming solar radiation at the top of the atmosphere for each obliquity. Black, red and blue symbols correspond to annual mean, DJF, and JJA means, respectively. Positive values indicate higher insolation at the equator. (For interpretation of the references to color in this figure legend, the reader is referred to the web version of this article.)

$0.064\,K^{-1}$. Stephens (1990) suggests $0.1 \leq r/(1+\lambda) \leq 0.3$ where r is the relative humidity and λ the atmospheric scale height divided by the scale height of the water vapor.

3. Results

In the following sections, we analyse the atmospheric variables that determine the habitability of a planet. We measure these variables in the Northern hemisphere using the meteorological definition for each season as a three months period: summer as June, July, August mean (JJA) corresponding to the period of time when the northern hemisphere faces the star and winter as December, January, February mean (DJF), as the period of time when the southern hemisphere faces the star. We also use the average of the 12 months as the annual mean (ANN).

3.1. Global mean surface temperature

A direct effect of raising the obliquity is an increase in the global mean annual surface temperature (T_{glob}). Fig. 1 shows a mere 9 K increase in the global temperature for such large obliquity variations. This suggests that both the ocean and the atmosphere are very efficient in redistributing the incoming solar radiation. We observe this especially in aquaplanets with high obliquities because they have surface temperatures above freezing throughout the year even when the insolation produces strong seasonal variations as the winter hemisphere is in complete darkness.

Latitudinal and interannual variations from the mean T_{glob} are largest at $\delta = 30^\circ$ (boxplot in Fig. 1), decreasing gradually towards $\delta = 52.5^\circ$. T_{glob} changes with obliquity following the empirical expression:

$$T_{glob} = -1.55 \times 10^4\, \delta^{-2.2} + 305.5 \qquad (3)$$

where T_{glob} is the annual global surface temperature in K and δ represents the obliquity in degrees.

The total amount of solar radiation arriving at the top of the atmosphere does not vary in our experiments, but it is the latitudinal distribution that changes. We will discuss this in the following section.

3.2. Incoming solar radiation distribution

The equator to pole difference of the incident radiation at the top of the atmosphere (ΔR), as defined in Eq. (1), decreases when obliquity increases.

Fig. 2 shows that in the annual mean the equator receives more insolation than the polar region for obliquities below $\delta = 54^\circ$. The opposite occurs above this obliquity.

Although the annual insolation curve is almost flat for $\delta = 54^\circ$, the seasonal ΔR goes from $-208\,W\,m^{-2}$ in summer to $+335\,W\,m^{-2}$ in winter. Overall, seasonal variations are smallest for $\delta = 30^\circ$, and largest for $\delta = 90^\circ$, when the polar regions receive as much as $R_{pol} = 726\,W\,m^{-2}$ during summer (compared to about $R_{pol} = 374\,W\,m^{-2}$ for $\delta = 30^\circ$). Values at the equator remain between $+420\,W\,m^{-2}$ (for $\delta = 30^\circ$) to $+334\,W\,m^{-2}$ (for $\delta = 90^\circ$).

In winter, as the obliquity increases, ΔR decreases linearly. Its value goes from $+382\,W\,m^{-2}$ to $+280\,W\,m^{-2}$, this is about $+1.7\,W\,m^{-2}$ by degree of obliquity. Polar regions receive $\approx 0\,W\,m^{-2}$ in winter maintaining the positive values of ΔR. In summer, ΔR decreases at a larger rate going from $+46\,W\,m^{-2}$ to $-392\,W\,m^{-2}$.

The atmosphere intervenes on how the incoming radiation reaches the surface, partitioning the solar energy into three components that we present in its global mean: Absorbed Solar Radiation at the surface (ASR), Absorbed Solar Radiation in the atmosphere (ASRa) and Outgoing Solar Radiation at the top of the atmosphere (OSR) shown in Fig. 3.

Oceanic albedo, with its low reflectivity, allows most of the solar radiation to be absorbed by the surface (ASR), as seen in Fig. 3. When the obliquity increases, ASR changes from $175\,W\,m^{-2}$ to $187\,W\,m^{-2}$. The areas of ASRa and OSR in Fig. 3 have similar size because the cloud cover (CC) is about 50%, reaching 54% at $\delta = 30^\circ$ and 48% at $\delta = 90^\circ$. ASRa increases between $73\,W\,m^{-2}$ and $76\,W\,m^{-2}$ and OSR decreases from $93\,W\,m^{-2}$ to $78\,W\,m^{-2}$. The changes in the partitioning of solar radiation are however not a clear function of obliquity. For $30^\circ \leq \delta \leq 52.5^\circ$ the mean values of ASR, ASRa and OSR are constant: $175\,W\,m^{-2}$, $250\,W\,m^{-2}$ and $90\,W\,m^{-2}$ respectively.

At $\delta = 52.5^\circ$, the atmosphere increases the absorption of solar radiation. OSR starts decreasing and ASR increases. CC changes the solar radiation distribution. Fig. 3 shows a mean CC between 50% and 60%. The aquaplanet with $\delta = 30^\circ$ presents the largest latitudinal and interannual variations, with a mean value of 55%. CC then

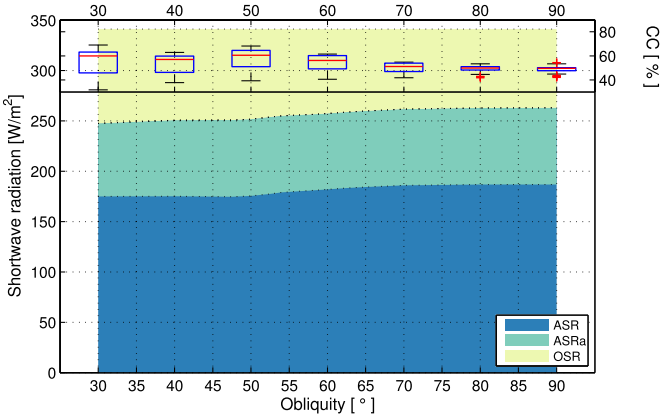

Fig. 3. Global annual mean partitioning of solar radiation for each obliquity. Blue indicates the Absorption of Solar Radiation at the surface (ASR), green is the Absorption of Solar Radiation by the atmosphere (ASRa) and yellow is the Outgoing Solar Radiation at the top of the atmosphere (OSR). Boxplots show the statistics for annual mean cloud cover (CC), about its latitudinal and interannual variations. (For interpretation of the references to color in this figure legend, the reader is referred to the web version of this article.)

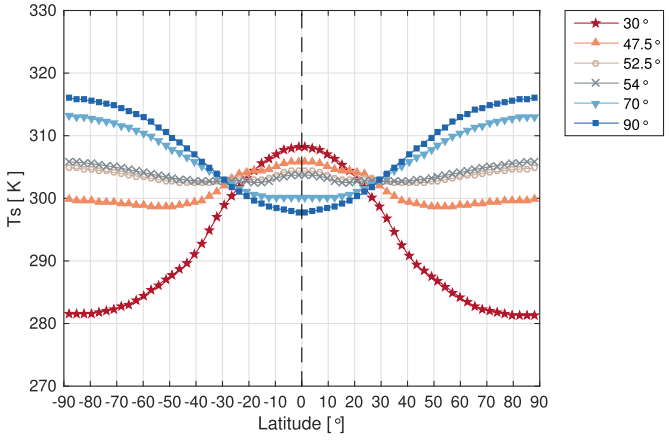

Fig. 4. Latitudinal distribution of the annual mean surface temperature T_s, for some representative cases of simulated aquaplanets (colour lines).

increases to about 60% for $\delta = 52.5°$. This rise in CC maintains the ASR almost constant for this obliquity range. Above 52.5° global CC decreases, reaching mean values below 50% at $\delta = 90°$. Latitudinal and interannual variations also decrease for the high obliquity aquaplanets. The reduction of CC produces smaller solar reflection and larger absorption of solar radiation by the surface.

3.3. Atmospheric water vapor

Our Earth-like aquaplanets simulations have a blackbody equilibrium temperature (T_{eq}) of 274 K. However, the annual mean global surface temperature (T_{glob}) varies between 296 K and 305 K (Fig. 1) for changing obliquity. This rise of 22 K to 30 K from T_{eq} is a result of the atmosphere and its greenhouse effect causing T_{glob} to be warmer than T_{eq} in all our experiments.

T_{glob} increases because of atmospheric water vapor content, the main cause responsible for the greenhouse effect in these aquaplanets. The global mean precipitable water content in the atmosphere (*PWV*) increases almost twofold from $\delta = 30°$ to $\delta = 90°$, following the Clausius-Clapeyron relation (Supplementary Fig. 1).

We applied the same algorithm used by Stephens (1990) to predict *PWV* as a function of SST. The best fit for our aquaplanets is obtained for $r/(1+\lambda) = 0.21$ (Supplementary Fig. 1). Although the behavior is somewhat steeper at the highest temperatures ($80° \leq \delta \leq 90°$). We found for the aquaplanets a slightly higher value than the measurements given for the Earth by Stephens (1990), but well within the limits of the parameters they proposed.

3.4. Latitudinal distribution of surface temperature

Polar amplification and temperatures above freezing are the main features in the latitudinal distribution of annual mean surface temperature (T_s) as the climate changes from cold to warm poles (see Fig. 4). We identify two regimes with similar behavior delimited by $\delta = 52.5°$. Below this obliquity, the equator is warmer than the poles. Over $\delta = 52.5°$ polar regions are warmer, as one would expect from the insolation distribution. The annual mean temperature has a constant value of 302 K at latitudes $\pm 30°$, except in the aquaplanet with $\delta = 30°$, which is colder at these latitudes. We observe the smallest latitudinal temperature gradient in the aquaplanet with $\delta = 52.5°$, although at $\delta = 54°$ the latitudinal insolation curve is flat.

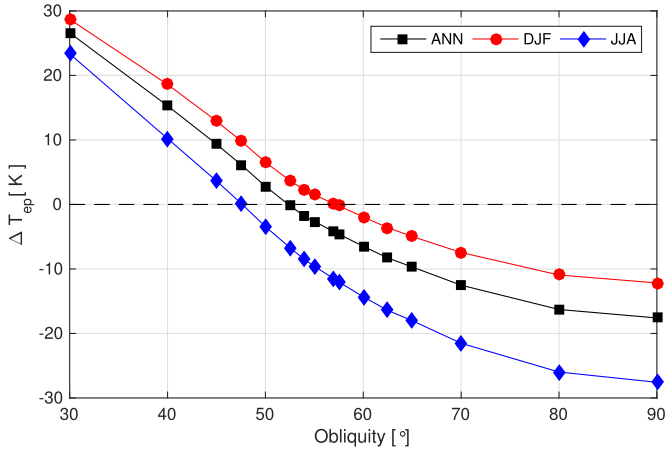

Fig. 5. Equator to pole difference of surface temperature (ΔT) for each obliquity. Black, red and blue symbols correspond to annual, DJF and JJA means, respectively. Positive values indicate higher temperatures at the equator. (For interpretation of the references to color in this figure legend, the reader is referred to the web version of this article.)

Surface temperature between Equator and Poles range between 303.7 K and 305.8 K at $\delta = 54°$; 302.1 K to 309 K at $\delta = 60°$ and 297.8 K to 316 K at $\delta = 90°$. Comparison with previous studies indicates these surface temperatures have a similar range as Linsenmeier et al. (2015) when $\delta = 60°$ and 90°, but are higher in our case than Ferreira et al. (2014) when $\delta = 54°$ and 90°.

Fig. 5 shows that the largest ΔT is found for $\delta = 30°$, for both the annual and seasonal means. ΔT decreases towards zero for $\delta = 52.5°$, and increases again for higher obliquities. $\Delta T = 0$ K occurs in the annual mean at $\delta = 52.5°$ and seasonally at $\delta = 47.5°$ (summer) and $\delta = 57.5°$ (winter), being thus the planets with the weakest synoptic scale atmospheric activity.

With increasing obliquity, ΔT does not decrease linearly as in ΔR , instead ΔT decreases at a larger rate. Comparing $\delta = 30°$ with $\delta = 90°$, ΔT decreases 59% in winter, increases 18% in summer and decreases by 33%, annually. $\Delta T < 0$ K indicates that the poles are warmer than the equator.

3.5. Atmospheric circulation

The differential insolation produces latitudinal temperature gradients in the atmosphere that are in thermal gradient balance with zonal westerly winds. The tropospheric temperature and wind structures sustain the large scale atmospheric overturning circula-

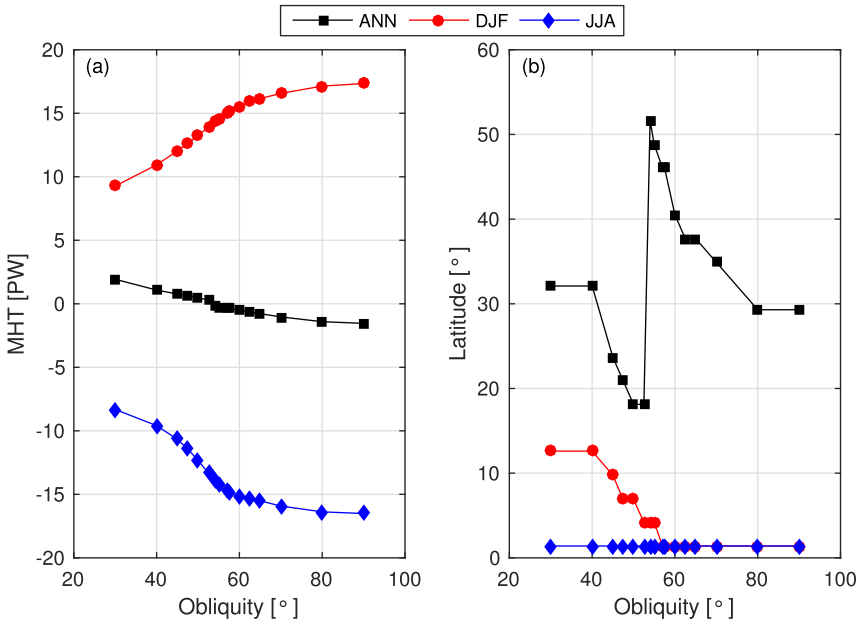

Fig. 6. (a) Maximum value of MHT for each obliquity, (b) position of the maximum, in winter (DJF, red circles), summer (JJA, blue diamonds) and annual mean (black squares). Positive (negative) values indicate northward (southward) transport. (For interpretation of the references to color in this figure legend, the reader is referred to the web version of this article.)

tion (Hadley cells; Held and Hou, 1980), associated baroclinic instabilities and storm-tracks that transport heat from warmer to colder regions in the atmosphere. Supplementary Fig. 2 shows two vertical cross section of zonal (east to west) winds for $\delta = 45^\circ$ and 65°, as well as the jet stream intensity and position at 200 hPa (the altitude of maximum jet streams)[1].

Strongest winds occur around $\pm 30^\circ$ for $\delta = 45^\circ$ (Supplementary Fig. 2a); this is the case for aquaplanets with obliquities below 50°. As obliquity increases, the poles start receiving more insolation than the equator in the annual mean, the temperature gradients decrease, and the jet streams decrease their intensity. At the same time, easterly winds at equatorial latitudes start to appear. From $\delta = 50^\circ$ onwards, easterly winds develop at upper levels, increasing in speed as the reversed meridional temperature gradient increases, and intrudes from the summer hemisphere into the winter hemisphere (negative magnitudes in supplementary Fig. 2b). At high obliquity, the meridional temperature gradients for the winter hemisphere throughout the troposphere are very small because the complete hemisphere receives little insolation from the top and is uniformly heated from below by the ocean (see Ferreira et al., 2014). Thus the large values seen in supplementary Fig. 2c reflect inter-hemispheric temperature gradients.

The large-scale atmospheric overturning circulation is also affected by these large seasonal changes at high obliquity. The seasonal Hadley cell is a thermally direct circulation predominantly in the winter hemisphere, with rising motion at its equatorial flank (summer hemisphere) and descent in the winter hemisphere. However a narrower and weaker cell is present in the summer hemisphere. Supplementary Fig. 3 shows the latitudinal extent of the Hadley cell at 500 hPa, depicted by the mass stream function. From $\delta = 45^\circ$ the narrower summer hemisphere cell disappears completely and the main cell becomes descending wider well into the summer hemisphere.

In the annual mean, the mid-latitude overturning circulation (Ferrell cells; Kuo, 1956) increases its height and moves to the Equator affecting the shape of Hadley cells. This change in Hadley cells height affects the behavior of the Inter Tropical Convergence Zone (ITCZ). As we can see in supplementary Fig. 4 maximum precipitation in the ITCZ in the annual mean decreases related to the intensity (Supplementary Fig. 5) and height of the Hadley cell.

Finally, we show the atmospheric meridional heat transport (MHT) resulting from these large-scale circulation changes in Fig. 6, including the latitude of the maximum MHT. The MHT is calculated using the DB method (Donohoe and Battisti, 2012). In the annual mean the absolute value of MHT is largest for $\delta = 30^\circ$, decreases to a minimum value for $\delta = 52.5^\circ$ and then increases again. The direction of transport is down the temperature gradient (from warm to cold regions) and hence towards the pole for $30^\circ \leq \delta \leq 54^\circ$ (positive values). Then it reverses direction and moves towards the equator (negative values, Fig. 6a and b). For high obliquities, it is the summer hemisphere that drives the heat transport. As we saw earlier, the flat meridional temperature structure in the winter hemisphere reduces the winds and hence the eddy components of the heat transport. During Northern Hemisphere winter (JJA) the Southern Hemisphere transports heat into the Northern hemisphere. The largest values are near the equator (Fig. 6b).

3.6. Habitability: Wet bulb temperature

Our obliquity experiments result in aquaplanets with temperate surface temperatures which maintain liquid water during the year. Having fulfilled this condition, a step further is to define an atmospheric indicator of habitability, since high temperatures could also limit the development of complex life, especially in Earth-like atmospheres, with a high level of humidity.

We use the wet bulb temperature (T_w; Stull, 2011) which relates relative humidity (%) and air temperature (°C), as an atmospheric indicator for evaluating the latitudinal extent of habitability.

Even when extremophiles can survive in regions with high temperatures, we define the habitable range as $0^\circ \leq T_w \leq 35^\circ$; because complex life such as mammals can not survive above this temperature. Fig. 7 shows the percentage of months in which each region falls within this range. Obliquities below $\delta = 54^\circ$ are 100% habitable. Above $\delta = 70^\circ$, year-long habitability is only possible in the

[1] Figures for other obliquities are available upon request to the author.

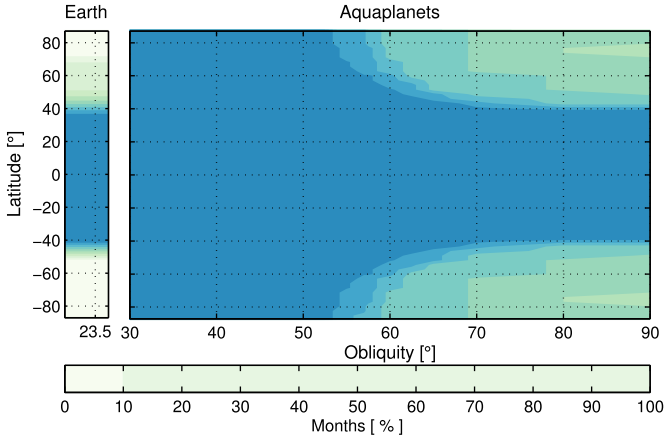

Fig. 7. Latitudinal distribution of monthly percentage of zonal mean habitability of each aquaplanet with all seasons ice free conditions. Habitability is defined by a Tw temperature range of $0°C \leq T_w \leq 35°C$.

region between latitudes $\pm 40°$, poleward of 40° latitude the humidity increases such to reduce habitability to half of the year.

Fig. 7 also shows that aquaplanets with obliquities above 30° are more habitable than our planet. We perform a true Earth simulation with continents and $\varepsilon = 0$, to compare the latitudinal extent of habitability. On Earth, only the latitudes between $\pm 40°$ are 100% habitable under defined range of T_w, but in this case humidity and temperature decrease, diminishing habitability poleward. In the Northern hemisphere continents increase T_w maintaining this region half of the year habitable.

The analysis for habitability here presented corresponds to experiments that are ice-free for all months. In the case of either seasonal ice or snowball-earth conditions this would clearly alter the efficiency of latitudinal energy transport and could therefore lead to climatic instability (e.g. Kilic et al., 2017).

4. Conclusions

We performed 16 aquaplanet experiments varying obliquity from 30° to 90° with finer sampling around 55°. Although the total amount of solar radiation that reaches the top of the atmosphere is the same for all experiments, changing obliquity has several effects.

Increasing obliquity produces a progressive change in the latitudinal insolation distribution from low to high obliquities. In the annual mean the insolation is the same at the equator and poles at $\delta = 54°$, acting as a pivot that divides the insolation distribution into two ranges: higher insolation at equator ($30° \leq \delta < 54°$), and higher insolation at the poles ($54° < \delta \leq 90°$).

High obliquity increases seasonality. Both winter and summer become more extreme as a larger proportion of the hemisphere stays in darkness, and insolation increases its values up to 700 $W\,m^{-2}$ in the summer hemisphere.

The Earth-like atmospheric composition of the aquaplanets determines that the surface absorbs most of the insolation; a fraction of this radiation is reflected back into space, and another fraction is absorbed by the atmosphere, depending on cloud cover (CC). The radiation absorbed by the surface reaches its maximum value at $\delta = 90°$, while CC and the reflected radiation are minima. Solar radiation absorbed by the atmosphere stays constant in all our experiments.

The overall effect on the winter hemisphere is that the meridional temperature structure becomes flat, with all the consequences on the large-scale circulation that this implies.

In terms of the large-scale atmospheric circulation, that redistributes the differential solar energy input, 54° is confirmed as the obliquity where a transition occurs and the complete evolution of the two regimes is analysed. For obliquities below 54°, when the equator receives more insolation than the poles, the large-scale circulation follows the known Earth's dynamics. The latitudinal temperature gradient determines tropospheric westerly jet streams together with the Hadley and Ferrel cells and maximum precipitation in the tropics (the ITCZ), and the MHT is from low to high latitudes. As the latitudinal temperature gradients in the annual mean decrease close to obliquities of 54°, the circulation is less vigorous, with weaker overturning cells and jet streams and hence minimum MHT. However, because there are still large seasonal variations, the circulation does not shutdown as one could expect. For obliquities above 54°, the latitudinal temperature gradient reverses and this has various important impacts. Easterly winds appear in the tropics of the higher troposphere due to this reversed temperature gradient especially in the summer hemisphere (also found in Linsenmeier et al. (2015)). On the other hand, the temperature structure of the winter hemisphere at high obliquity becomes increasingly flat, because from the top less and less insolation is received, and from the bottom (ocean) a constant amount of heat is received so that none of the aquaplanets freeze even at $\delta = 90°$. This regulating effect of the ocean is not an artifact of our modelling setup (slab ocean), but was also found in experiments with a fully dynamical ocean coupled to the atmosphere (Ferreira et al., 2014). As in their experiment, the ocean in our simulations acts as an reservoir releasing the stored heat into the atmosphere through convection, highlighting the importance of a liquid ocean in regulating the climate of a planet. We observe this effect in the global mean temperature that changes only 9 K as the obliquities increases from 30° to 90°.

These aquaplanets fulfill the basic habitability condition because they maintain a liquid ocean during the year. Yet, high temperatures raise the water vapor content in the atmosphere and some complex life such as mammals can not survive in regions where temperature and humidity are high. We use the wet bulb temperature to relate these variables as an atmospheric index of habitability.

Habitability maps show that aquaplanets at high obliquity are more habitable than Earth under the same orbital conditions even when one of the hemispheres is in total darkness. Aquaplanets keep this completely latitudinal habitability during the year for obliquities under 54°. Above this value, habitability decreases toward the poles being half of the year habitable. These high obliquity aquaplanets maintain their 100% habitability between $\pm 40°$ Latitude. Comparing with the Earth, this is the region where our planet is completely habitable, and continents help to increase habitability toward the colder regions.

Acknowledgements

This research was partially financed by CONICYT grant no. 21110653, FONDECYT project no. 1171773, NC120066, and Center for Climate Science and Resiliency $(CR)^2$, FONDAP-CONICYT n. 15110009.

Thanks to Frank Lunkeit and Edilbert Kirk, developers of PlaSim for helping me to use the model.

Supplementary material

Supplementary material associated with this article can be found, in the online version, at 10.1016/j.icarus.2018.01.002.

References

Berger, A., Loutre, M., 1991. Insolation values for the climate of the last 10 million years. Quat. Sci. Rev. 10 (4), 297–317. doi:10.1016/0277-3791(91)90033-Q.

Bills, B.G., 1990. The rigid body obliquity history of Mars. J. Geophys. Res. 95 (B9), 14137. doi:10.1029/JB095iB09p14137.
Dobrovolskis, A.R., Harris, A.W., 1983. The obliquity of Pluto. Icarus 55 (2), 231–235. doi:10.1016/0019-1035(83)90077-5.
Donohoe, A., Battisti, D.S., 2012. What determines meridional heat transport in climate models? J. Clim. 25 (11), 3832–3850. doi:10.1175/JCLI-D-11-00257.1.
Ferreira, D., Marshall, J., O'Gorman, P.A., Seager, S., 2014. Climate at high-obliquity. In: Icarus, 243, pp. 236–248. doi:10.1016/j.icarus.2014.09.015.
Fraedrich, K., Jansen, H., Kirk, E., Luksch, U., Lunkeit, F., 2005. The planet simulator: towards a user friendly model. Meteorol. Z. 14 (3), 299–304. doi:10.1127/0941-2948/2005/0043.
Held, I.M., Hou, A.Y., 1980. Nonlinear axially symmetric circulations in a nearly inviscid atmosphere. J. Atmos. Sci. 37 (3), 515–533. doi:10.1175/1520-0469(1980)037⟨0515:NASCIA⟩2.0.CO;2.
Hoffman, P.F., 1998. A Neoproterozoic Snowball Earth. Science 281 (5381), 1342–1346. doi:10.1126/science.281.5381.1342.
Imbrie, J., Berger, A., Boyle, E.A., Clemens, S.C., Duffy, A., Howard, W.R., Kukla, G., Kutzbach, J., Martinson, D.G., McIntyre, A., Mix, A.C., Molfino, B., Morley, J.J., Peterson, L.C., Pisias, N.G., Prell, W.L., Raymo, M.E., Shackleton, N.J., Toggweiler, J.R., 1993. On the structure and origin of major glaciation cycles 2. The 100,000-year cycle. Paleoceanography 8 (6), 699–735. doi:10.1029/93PA02751.
Jenkins, G.S., 2000. Global climate model high-obliquity solutions to the ancient climate puzzles of the Faint-Young Sun Paradox and low-altitude Proterozoic Glaciation. J. Geophys. Res. 105 (D6), 7357–7370. doi:10.1029/1999JD901125.
Kasting, J.F., 1988. Runaway and moist greenhouse atmospheres and the evolution of Earth and Venus. Icarus 74 (3), 472–494. doi:10.1016/0019-1035(88)90116-9.
Kilic, C., Raible, C., Stocker, T., 2017. Multiple climate states of habitable exoplanets: the role of obliquity and irradiance. Astrophys. J. 844 (147), 13pp. doi:10.3847/1538-4357/aa7a03.
Kopparapu, R.K., Ramirez, R., Kasting, J.F., Eymet, V., Robinson, T.D., Mahadevan, S., Terrien, R.C., Domagal-Goldman, S., Meadows, V., Deshpande, R., 2013. Habitable Zones around main-sequence stars: new estimates. Astrophys. J. 765 (2), 131. doi:10.1088/0004-637X/765/2/131.
Kuo, H.-L., 1956. Forced and free meridional circulations in the atmosphere. J. Meteorol. 13 (6), 561–568. doi:10.1175/1520-0469(1956)013⟨0561:FAFMCI⟩2.0.CO;2.
Laskar, J., Joutel, F., Robutel, P., 1993. Stabilization of the Earth's obliquity by the Moon. Nature 361 (6413), 615–617. doi:10.1038/361615a0.
Laskar, J., Robutel, P., 1993. The chaotic obliquity of the planets. Nature 361 (6413), 608–612. doi:10.1038/361608a0.
Linsenmeier, M., Pascale, S., Lucarini, V., 2015. Climate of Earth-like planets with high obliquity and eccentric orbits: implications for habitability conditions. Planet Space Sci. 105, 43–59. doi:10.1016/j.pss.2014.11.003.
North, G.R., Erukhimova, T.L., 2009. Atmospheric Thermodynamics. Cambridge University Press, Cambridge doi:10.1017/CBO9780511609695.
Payne, R.E., 1972. Albedo of the Sea Surface. J. Atmos. Sci. 29 (5), 959–970. doi:10.1175/1520-0469(1972)029⟨0959:AOTSS⟩2.0.CO;2.
Sagan, C., Mullen, G., 1972. Earth and Mars: evolution of atmospheres and surface temperatures. Science 177 (4043), 52–56. doi:10.1126/science.177.4043.52.
Sherwood, S.C., Huber, M., 2010. An adaptability limit to climate change due to heat stress. Proc. Natl. Acad. Sci. 107 (21), 9552–9555. doi:10.1073/pnas.0913352107.
Spiegel, D.S., Menou, K., Scharf, C.A., 2008. Habitable climates. Astrophys. J. 681 (2), 1609–1623. doi:10.1086/588089.
Spiegel, D.S., Menou, K., Scharf, C.A., 2009. Habitable climates: the influence of obliquity. Astrophys. J. 691 (1), 596–610. doi:10.1088/0004-637X/691/1/596.
Stephens, G.L., 1990. On the relationship between water vapor over the oceans and sea surface temperature. J. Clim. 3 (6), 634–645. doi:10.1175/1520-0442(1990)003⟨0634:OTRBWV⟩2.0.CO;2.
Stull, R., 2011. Wet-bulb temperature from relative humidity and air temperature. J. Appl. Meteorol. Climatol. 50 (11), 2267–2269. doi:10.1175/JAMC-D-11-0143.1.
Sugiyama, M., Stone, P.H., Emanuel, K.A., 2005. The role of relative humidity in radiative convective equilibrium. J. Atmos. Sci. 62 (6), 2001–2011. doi:10.1175/JAS3434.1.
Touma, J., Wisdom, J., 1993. The chaotic obliquity of Mars.. Science (New York, N.Y.) 259 (5099), 1294–1297. doi:10.1126/science.259.5099.1294.
Ward, W.R., 1974. Climatic variations on Mars: 1. Astronomical theory of insolation. J. Geophys. Res. 79 (24), 3375–3386. doi:10.1029/JC079i024p03375.
Williams, D.M., Kasting, J.F., 1997. Habitable planets with high obliquities. Icarus 129 (1), 254–267. doi:10.1006/icar.1997.5759.
Williams, D.M., Pollard, D., 2003. Extraordinary climates of Earth-like planets: three-dimensional climate simulations at extreme obliquity. Int. J. Astrobiol. 2 (1), 1–19. doi:10.1017/S1473550403001356.
Williamson, D.L., Blackburn, M., Nakajima, K., Ohfuchi, W., Takahashi, Y.O., Hayashi, Y.-Y., Nakamura, H., Ishiwatari, M., McGregor, J.L., Borth, H., Wirth, V., Frank, H., Bechtold, P., Wedi, N.P., Tomita, H., Satoh, M., Zhao, M., Held, I.M., Suarez, M.J., Lee, M.-I., Watanabe, M., Kimoto, M., Liu, Y., Wang, Z., Molod, A., Rajendran, K., Kitoh, A., Stratton, R., 2013. The Aqua-Planet Experiment (APE): response to changed meridional SST profile. J. Meteorol. Soc. Jpn. Ser. II 91A (0), 57–89. doi:10.2151/jmsj.2013-A03.